Stellar modelling of Spica, a high-mass spectroscopic binary with a beta Cep variable primary component

Tkachenko, A.; Matthews, J.M.; Aerts, C.; Pavlovski, Krešimir; Papics, P.I.; Zwintz, K.; Cameron, C.; Walker, G.A.H.; Kuschnig, R.; Degroote, P.; ...

Stellar modelling of Spica, a high-mass spectroscopic binary with a β Cep variable primary component

A. Tkachenko,[1]⋆† J. M. Matthews,[2] C. Aerts,[1,3] K. Pavlovski,[4] P. I. Pápics,[1]‡
K. Zwintz,[5] C. Cameron,[2,6] G. A. H. Walker,[2] R. Kuschnig,[7] P. Degroote,[1]
J. Debosscher,[1] E. Moravveji,[1] V. Kolbas,[4] D. B. Guenther,[8] A. F. J. Moffat,[9]
J. F. Rowe,[10] S. M. Rucinski,[11] D. Sasselov[12] and W. W. Weiss[7]

[1]*Instituut voor Sterrenkunde, KU Leuven, Celestijnenlaan 200D, B-3001 Leuven, Belgium*
[2]*Department of Physics and Astronomy, University of British Columbia, 6224 Agricultural Road, Vancouver, BC V6T 1Z1, Canada*
[3]*Department of Astrophysics, IMAPP, Radboud University Nijmegen, NL-6500 GL Nijmegen, the Netherlands*
[4]*Department of Physics, University of Zagreb, Bijenička cesta 32, 10000 Zagreb, Croatia*
[5]*Institute for Astro- and Particle Physics, University of Innsbruck, Technikerstrasse 25/8, A-6020 Innsbruck, Austria*
[6]*Department of Mathematics, Physics & Geology, Cape Breton University, 1250 Grand Lake Road, Sydney, NS B1P 6L2, Canada*
[7]*University of Vienna, Institute of Astronomy, Türkenschanzstrasse 17, AT-1180 Vienna, Austria*
[8]*Department of Astronomy and Physics, St Marys University, Halifax, NS B3H 3C3, Canada*
[9]*Départment de physique, Université de Montréal, C.P.6128, Succ. Centre-Ville, Montréal, QC H3C 3J7, Canada*
[10]*NASA-Ames Research Park, MS-244-30, Moffett Field, CA 94035, USA*
[11]*Department of Astronomy & Astrophysics, University of Toronto, 50 St George Street, Toronto, ON M5S 3H4, Canada*
[12]*Harvard–Smithsonian Center for Astrophysics, 60 Garden Street, Cambridge, MA 02138, USA*

ABSTRACT

Binary stars provide a valuable test of stellar structure and evolution, because the masses of the individual stellar components can be derived with high accuracy and in a model-independent way. In this work, we study Spica, an eccentric double-lined spectroscopic binary system with a β Cep type variable primary component. We use state-of-the-art modelling tools to determine accurate orbital elements of the binary system and atmospheric parameters of both stellar components. We interpret the short-period variability intrinsic to the primary component, detected on top of the orbital motion both in the photometric and spectroscopic data. The non-local thermodynamic equilibrium based spectrum analysis reveals two stars of similar atmospheric chemical composition consistent with the present-day cosmic abundance standard. The masses and radii of the stars are found to be 11.43 ± 1.15 M$_\odot$ and 7.21 ± 0.75 M$_\odot$, and 7.47 ± 0.54 R$_\odot$ and 3.74 ± 0.53 R$_\odot$ for the primary and secondary, respectively. We find the primary component to pulsate in three independent modes, of which one is identified as a radial mode, while the two others are found to be non-radial, low degree l modes. The frequency of one of these modes is an exact multiple of the orbital frequency, and the $l = m = 2$ mode identification suggests a tidal nature for this particular mode. We find a very good agreement between the derived dynamical and evolutionary masses for the Spica system to within the observational errors of the measured masses. The age of the system is estimated to be 12.5 ± 1 Myr.

Key words: binaries: spectroscopic – stars: fundamental parameters – stars: individual: α Virginis – stars: oscillations – stars: variables: general.

1 INTRODUCTION

Spectroscopic binary stars provide a valuable test of stellar structure and evolution models since accurate, model-independent dynamical masses can be measured for the individual stellar components of a binary. Moreover, an existence of pulsating stars in binary

⋆ E-mail: andrew@ster.kuleuven.be
† Postdoctoral Fellow of the Research Foundation Flanders.
‡ Postdoctoral Fellow of the Research Foundation Flanders.

systems allows the confrontation of the dynamical masses with those obtained from the asteroseismic analysis. Since the latter masses are model-dependent, pulsators in binary systems provide a test of the theory of stellar evolution and oscillations. Apart from that, massive stars in binary systems are known to suffer from the so-called mass discrepancy problem, which is important to investigate in the context of improving the current theories of stellar structure and evolution. The term mass discrepancy was first introduced by Herrero et al. (1992) and in its original formulation refers to the disagreement between the spectroscopic and evolutionary masses of the star. The evolutionary mass is the one estimated by fitting evolutionary tracks to a position of the star in the Hertzsprung–Russel or T_{eff}–$\log g$ Kiel diagram, whereas the spectroscopic mass stands for the stellar mass computed from the spectroscopically derived value of the surface gravity and from the radius of the star. The radius is in turn calculated from the absolute visual magnitude of the star and the (effective temperature dependent) integral of stellar flux over the wavelength (see Kudritzki 1980). Thus, the definition of the mass discrepancy by Herrero et al. (1992) has nothing to do specifically with binary systems but refers to massive stars in general. We keep on using the term mass discrepancy in application to binary systems throughout the paper, and warn the reader that we refer to the discrepancy between the evolutionary masses and those inferred from binary dynamics (dynamical masses).

This paper is the third in a series and concerns a detailed investigation of Spica, a short-period double-lined spectroscopic binary containing a massive star, where we address the above mentioned problems. In the two previous studies, the double-lined spectroscopic binary systems V380 Cyg (Tkachenko et al. 2014a) and σ Scorpii (Tkachenko et al. 2014b) have been investigated. The asteroseismic modelling of the primary component of σ Sco was largely successful leading to the mass and radius determination to precisions of 10 per cent or better, which is a factor of 3 more accurate than the corresponding values derived from the combined spectroscopic orbital and atmospheric parameters, and the interferometric orbital inclination angle (taken from North et al. 2007). We have found an evidence of the mass discrepancy for the secondary component of the binary, i.e. the evolutionary models suggest higher mass than the one inferred from the binary dynamics. The study of V380 Cyg benefited from the fact that it is an eclipsing system with space-based photometry available, thus the dynamical masses and radii of the individual stellar components could be derived to precisions approaching 1 per cent level. Both components of the binary were found to show significant discrepancy between the dynamical and evolutionary masses, leading us to the conclusion that the single star evolutionary models are inadequate for this particular system.

Spica ($V = 0.97$ mag, discovered to be a spectroscopic binary by Vogel 1890) is an important system to study in the context of testing the current theories of stellar structure and evolution for massive stars, which are way more uncertain than the models for lower mass stars. The more evolved primary component is also known to be an intrinsically variable star that belongs to the class of β Cep variables (Aerts, Christensen-Dalsgaard & Kurtz 2010, Chapter 2) and pulsates in pressure modes. As a consequence, the system was the subject of numerous studies addressing both the questions on configuration of the orbit as well as on the variability intrinsic to the primary component. For example, Shobbrook, Lomb & Herbison-Evans (1972) used both the newly obtained and historical radial velocity (RV) data to determine orbital parameters of the binary. The obtained solution was found to be in good agreement with the one reported by Herbison-Evans et al. (1971). Mathis & Odell (1973), Odell (1974)

have analyzed the Spica system by means theoretical models based on the masses, radii, and orbital elements derived by Herbison-Evans et al. (1971). Both studies reported the discrepancy between the observed and predicted by the models apsidal constant, which could (at least partially) be resolved by introducing an extra mixing (rotation or convective overshoot) in the inner regions of the star.

Despite the extensive investigations in the past, the oscillation behaviour of Spica is currently not well understood: several studies reported about irregular variability of the individual frequencies on short time-scales, and there is quite some diversity in the reported frequencies the Spica system was found to pulsate in (see Section 6 for an overview). The fact that the system is eccentric and the intrinsic pulsations of the more evolved component are in the range below 6 d^{-1} (69.4 μHz) makes it an interesting target to search for pulsations that are resonantly driven by the dynamic tide. These so-called tidally induced pulsations (Aerts et al. 2010, Chapter 2) have so far been detected in BA main-sequence stars with masses below 5 M$_\odot$ (e.g. Welsh et al. 2011; Thompson et al. 2012; Hambleton et al. 2013; Pápics et al. 2013) but never in early B-type stars. Should this type of stellar oscillation be found in either of the stellar components of the Spica system, it will be the first massive binary in which resonantly driven oscillations have been detected. Such a detection would make Spica an important test case for the evolution of massive stars in binary systems as the tidally induced pulsations are expected to play a significant role in angular momentum exchange between the orbit and the individual stellar components, and thus in the evolution of the orbital elements of the system with time.

Better observational constraints on the oscillation behaviour of Spica could be obtained if high-quality space-based were available for this star. Moreover, the system was also reported by Desmet et al. (2009) as possibly a grazingly eclipsing binary, so good quality observational data coupled to state-of-the-art analysis are required to detect a tiny eclipse signal, if present at all. A possible detection of the eclipses in the photometric data of the system could help to constrain the fundamental properties of the individual stellar parameters to a better precision than is currently available.

Overall, our study addresses several scientific questions at the same time. First of all, we aim at improving the understanding of the pulsational behaviour of the Spica system using and improved observational data set, including high-quality photometric observations from space combined with high-quality high-resolution ground-based spectroscopy (see Section 2). The orbital configuration of the system is determined in Sections 3 and 4, with a particular interest in whether the star could be a grazingly eclipsing system. We also perform a detailed (atmospheric) chemical composition analysis for both stellar components of the binary (Section 5), which particularly allows us to see whether a increased nitrogen abundance at the surface of the star due to rotational mixing applies to the Spica system as reported in the literature (e.g. Hunter et al. 2008; Brott et al. 2011). The intrinsic variability of the more massive component of the Spica system is explored in detail in Section 6. This includes detailed frequency analysis, identification of the individual pulsation modes from spectroscopic data, and a search for observational signatures of tidally induced pulsations. The possibility of detecting for the first time forced oscillations in a high-mass star (>5 M$_\odot$) defines the second scientific question we address in this study. Finally, we investigate the binary system in the context of the above-mentioned mass discrepancy problem by comparing the (spectroscopically inferred) positions of the individual stellar components in the T_{eff}–$\log g$ Kiel diagram with the evolutionary tracks (Section 7).

Table 1. List of the spectroscopic observations of Spica. JD is the Julian Date, *N* gives the number of spectra taken during the corresponding observational period.

Time period		*N*
Calendar date	JD (2 454 000+)	
19.03–01.04.2007	178–191	772
18.04–30.04.2007	208–220	798
22.07–30.07.2007	304–312	161
Total number of spectra:		**1731**

2 OBSERVATIONS AND DATA REDUCTION

We obtained 1731 high-resolution ($R = 50\,000$) high signal-to-noise ratio (S/N) spectra with the CORALIE spectrograph attached to the 1.2 m Euler Swiss Telescope (La Silla, Chile). The data were gathered in three different runs, in 2007 March, April, and July, and cover wide wavelength range between 381 and 681 nm. Table 1 gives the journal of our observations and lists calendar and Julian dates of the beginning and the end of the observing run, as well as the number of spectra that were obtained within each of the runs.

The spectroscopic data were reduced by means of a dedicated data reduction pipeline. The procedure included bias and stray-light subtraction, cosmic rays filtering, flat fielding, wavelength calibration by ThAr lamp, and order merging. Normalization to the local continuum has been done by fitting a cubic spline function through some tens of carefully selected continuum points. The whole normalization procedure as well as its implementation are described in more detail in Pápics et al. (2012).

Photometric data were gathered with the *MOST* space-based mission (Walker et al. 2003). The satellite is equipped with a 15-cm Rumak–Maksutov optical telescope feeding a CCD photometer. The Spica system was observed in the 'Fabry mode' of *MOST* (Walker et al. 2003), and was sampled using ∼30 s exposures over

a baseline of 22.92 d in 2007 March–April. The single point precision is of the order of 1–2 mmag; the complete light curve of the system is illustrated in Fig. 1 (top panel). For the analysis, the light curve was converted to a magnitude scale; a small, long-term instrumental trend has been removed by fitting a second-order degree polynomial to the entire data set.

The observational data set we analyse in this study is unique in the sense that (1) photometric data were obtained for the Spica system from space for the first time and are expected to provide much better constraints on the orbital configuration of the system and on the intrinsic variability of the individual stellar components; (2) the photometric data are complemented with extensive time series of ground-based spectroscopic observations that were taken during the same period of time. Detailed (combined) analysis of these data sets allows us to cross-match the photometrically inferred oscillation frequencies with those extracted from the spectroscopic data. The frequencies found in both data sets can be safely considered as intrinsic to the star and used for identification of the individual pulsation mode geometries based on well-sampled spectroscopic data. The output of such an analysis is one of the main pre-conditions for a detailed asteroseismic modelling of the star.

3 MODELLING THE LIGHT- AND RV-CURVE DATA

We used the method described in Pápics et al. (2013) to determine the RVs of both components from the composite observed spectra. Briefly, the method relies on the fitting of composite synthetic spectra to the observations, and comprises of two basic steps. First, a rough estimate of the spectroscopic parameters is made by fitting synthetic spectra to a single, high-quality observation taken at the orbital phase of largest RV separation, in a grid of $T_{\rm eff}$, $\log g$, $v \sin i$, and [M/H], in the range of several helium and metallic lines, as well as in the regions of Balmer H_β and H_γ line profiles. In the second
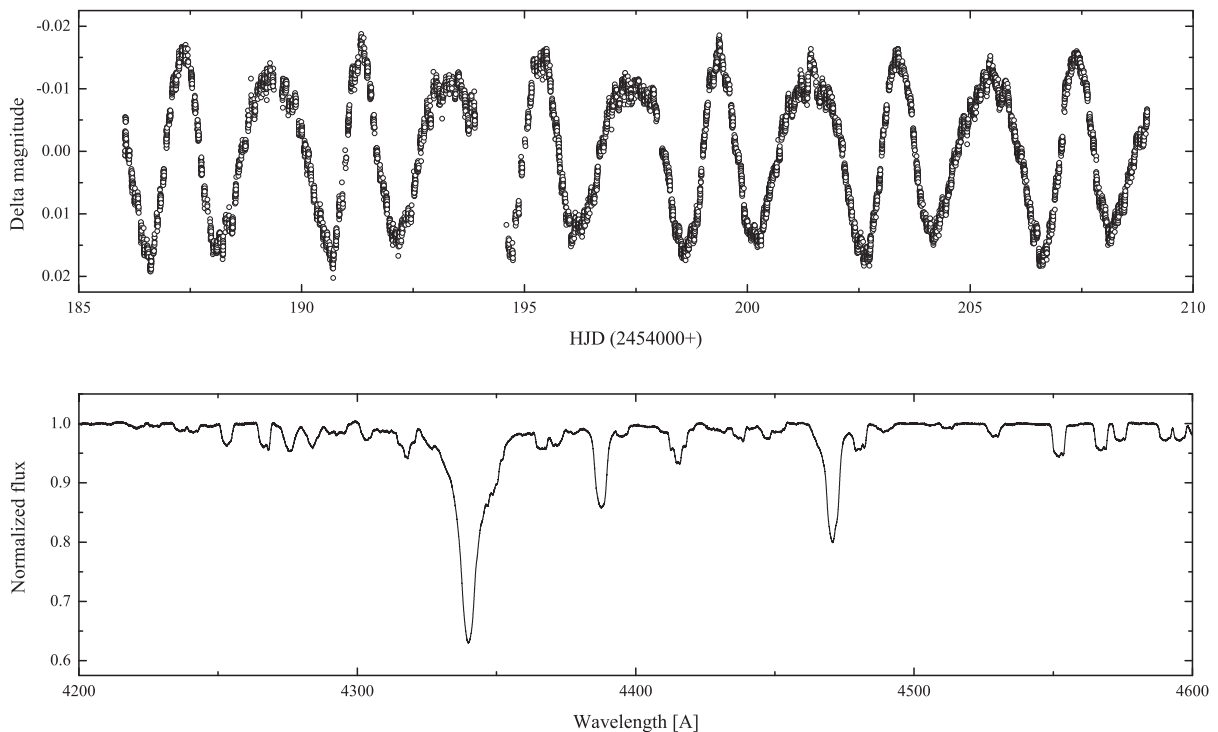

Figure 1. The *MOST* light curve (top) and a portion of the normalized, composite CORALIE spectrum (bottom) of Spica.

Table 2. Summary of the parameters for the final PHOEBE 2.0 solution of the *MOST* light- and CORALIE RV curves of Spica. A and B refer to the primary and secondary stars, respectively. The uncertainties on the parameters come from Markov Chain Monte Carlo simulations.

Parameter	Value	Uncertainty
Orbital period, P (d)	4.0145	0.0001
T_0 (HJD 24 54 000.+)	189.40	0.02
Orbital eccentricity[a], e	0.133	0.017
Longitude of periastron, ω (°)	255.6	12.2
Mass ratio[a], q	0.6307	0.023
Orbital inclination, i (°)	63.1	2.5
Orbital semimajor axis ($R_\odot$)	28.20	0.92
Systemic velocity, γ (km s^{-1})	−0.5	1.1
Rotation rates, A, B	2.0, 1.5	
Gravity darkening, A, B	1.0, 1.0	
Third light	0.0	
Star A potential	4.67	0.21
Star B potential	6.08	0.50
Fractional polar radii, A, B	0.250, 0.132	0.08, 0.05
Fractional equatorial radii, A, B	0.282, 0.134	0.09, 0.04
$T_{\rm eff}$ star A[a] (K)	25 300	500
$T_{\rm eff}$ star B (K)	20 585	850

[a]Adopted from spectroscopy

step, the atmospheric parameters are fixed to the values derived in the previous step, and RVs are determined by fitting composite synthetic spectra to all observed spectra leaving RVs of both components as variables. In our case, we could skip the first (rather time-consuming) step, and we used the parameters $T_{\rm eff}$ = 24 700/20 800, $\log g$ = 3.7/4.2, $v \sin i$ = 161/70, and [M/H] = 0.0/0.0 reported by Lyubimkov et al. (1995) for the primary/secondary component.

As pointed out by Harrington et al. (2009), the determination of the RVs of both binary components is complicated due to non-negligible line-profile variability (LPV) intrinsic to the primary component. In the result, the individual RVs of the primary measured as the first-order moment of the line profile may differ by up to 16 km s^{-1} from the average value, depending on the range of the profile that is used for the measurement (see fig. 3 in Harrington et al. 2009). Moreover, at the phases of close RV separation of the components, an additional uncertainty is added by the secondary to the RVs of the primary, but also the RVs of the secondary are affected by the LPV of the primary component. Both effects were clearly visible in our RVs, measured with the procedure outlined above. Thus, we used these RVs to provide initial guesses for the orbital parameters, but the final orbital solution was obtained by iterating between the light-curve fitting (using the most recent version of the PHOEBE2.0 code;[1] Degroote et al. 2013; Prša et al. 2013, see below) and the method of spectral disentangling (SPD, see Section 4). Such approach has an advantage in that it allows us to (at least partially) remove the degeneracy between the longitude of periastron (ω) and the eccentricity (e) of the system. In practice, the former parameter is better constrained from the light curve, whereas the eccentricity is better defined from the shape of the RV-curve of the system. This is exactly the reason why the eccentricity reported in Table 2 is mentioned as 'adopted from spectroscopy' but the ω value given in Table 3 is the one that comes from the light-curve solution.

The variability intrinsic to the primary component is also pronounced in the *MOST* light curve. To minimize the effect of this

Table 3. Orbital elements for Spica as derived by Herbison-Evans et al. (1971, indicated as H-E1971), Shobbrook et al. (1972, indicated as S1972), and in this study. Errors are given in parentheses in terms of last digits. Subscripts 1 and 2 refer to the primary and secondary component, respectively.

Param.	Unit	H-E1971	S1972	This study
P	d	4.014 55(3)	4.014 54(3)	4.0145(1)[b]
K_1	km s^{-1}	123.9(1.4)	124(4)	123.7(1.6)
K_2	km s^{-1}	198.8(1.5)	197(8)	196.1(1.6)
e		0.146(9)	0.14(3)	0.133(17)
ω[a]	degrees	138(6)	142(8)	255.6(12.2)[b]
T_0	HJD	2440 678.09(7)	2440 284.76(8)	2454 189.40(2)[b]

[a]The values measured at T_0.
[b]Fixed from the PHOEBE2.0 solution (see Section 3).

variability on the PHOEBE2.0 solution, the data were binned into 200 orbital phase bins of equal width. This number of phase bins was found to be optimal in the sense that it provided good enough sampling of the light curve and allowed to suppress the amplitude of the oscillations significantly.

A detached configuration of the system has been assumed in our calculations. Given the previously reported values for $v \sin i$ and radii of both components, as well as of the orbital inclination angle (e.g. Herbison-Evans et al. 1971; Lyubimkov et al. 1995), the synchronicity parameter was set to 2.0 and 1.5 for the primary and secondary star, respectively. Our final solution will show that this assumption is very close to reality. The gravity darkening coefficients were set to unity and the third light was fixed at zero. The effect of limb darkening is taken into account by means of the non-linear low introduced by Claret (2000). Unlike, e.g. the Wilson–Devinney approach (Wilson & Devinney 1971; Wilson 1979) where one, global set of coefficients is assumed to be valid on the entire star, PHOEBE2.0 takes into account the dependency of the coefficients on local conditions (effective temperature, gravity) on the star. This way, the limb darkening coefficients are not decoupled from the intensities anymore but are assumed to vary locally over the surface (Degroote et al. 2013).

The time of periastron passage (T_0), the eccentricity (e), the orbital inclination angle (i), the longitude of periastron (ω), the semimajor axis (a), the systemic velocity (γ), the dimensionless potentials ($\Omega_{1,2}$), and the effective temperature of the secondary ($T_{\rm eff,2}$) were set as adjustable parameters. The effective temperature of the primary ($T_{\rm eff,1}$) was initially fixed to the value of 24 700 K as derived by Lyubimkov et al. (1995), while the final solution was computed assuming our spectroscopically derived value of 25 300 K (see Section 5). Fixing the effective temperature of one of the stars is essential as only the temperature ratio of the two components can be constrained from white light photometry delivered by *MOST*. The final set of the parameters is given in Table 2, along with the uncertainties derived by means of the Markov Chain Monte Carlo simulations. We also provide fractional radii (stellar radii divided by the orbital semimajor axis) which are needed to compute the physical properties of the two stars. The system configuration is represented schematically at four different orbital phases in Fig. 2, while the quality of the fit of the phase-folded *MOST* light curve is illustrated in Fig. 3. As one can see (bottom-left panel in Fig. 2), the orbital inclination of Spica is such that it appears to be a nearly eclipsing system. Provided the error bars on the potentials of the two stars and the orbital inclination angle given in Table 2, Spica might indeed be a grazingly eclipsing binary system, where the more evolved primary partially blocks the light of the secondary component near phase 0.5, as suggested by Desmet et al. (2009).
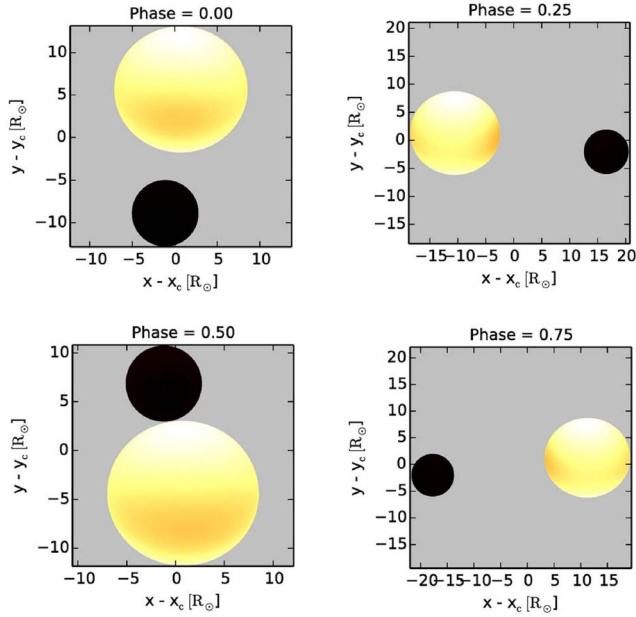
Figure 2. Schematic representation of the Spica binary system at four different orbital phases. Phase zero corresponds to the time of periastron passage. *X* and *Y* axes give the distance from the centre of mass in units of solar radii.
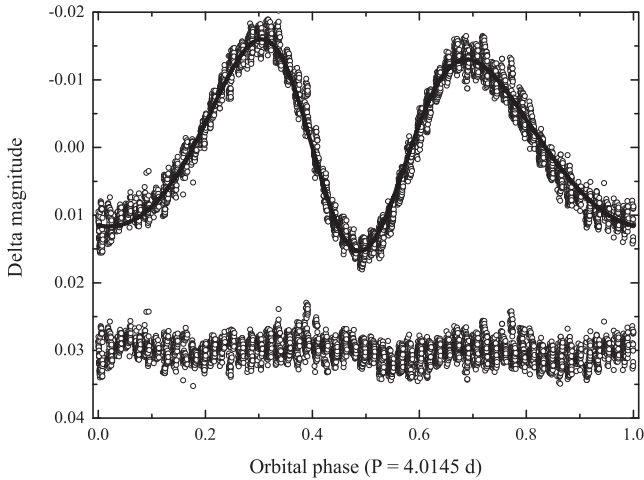

Figure 3. Best-fitting model (solid, thick line) to the phase-folded *MOST* light curve (open circles). The residuals have been shifted downwards by 0.03 mag for clarity.

Though the discovery of eclipses in this system would be an exciting result, it would hardly help better constrain orbital and physical parameters of the system.

A clear residual signal can be seen on top of the one due to the ellipsoidal variability of stars in the *MOST* light curve of Spica (see Fig. 3). This signal is clearly intrinsic to the star and will be discussed in Section 6 in more detail. We did not use the residual RVs obtained at this step for further analysis, as the more accurate spectroscopic information can be extracted from the original, composite spectra of a binary by subtracting the contribution of either of the binary components beforehand, using the corresponding disentangled spectrum (see Section 6).
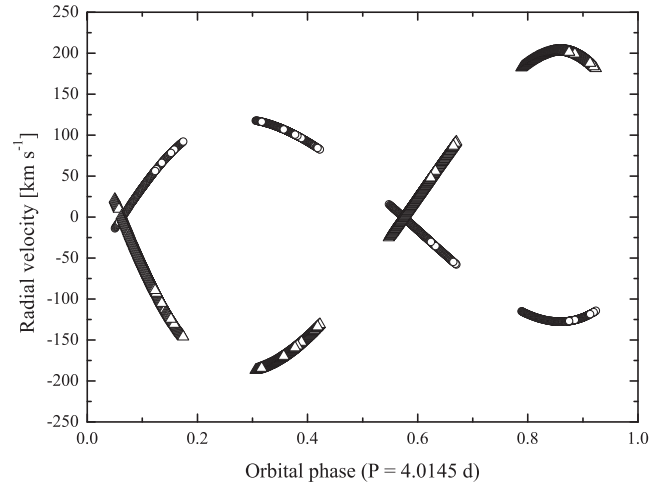
Figure 4. RVs of both binary components computed from the orbital solution reported in Table 3. The primary component is shown by open circles, whereas the secondary with open triangles.

4 SPECTRAL DISENTANGLING

To separate the spectra of two components, we used the method of SPD originally proposed by Simon & Sturm (1994), and formulated by Hadrava (1995) in Fourier space. The code we use is the FDBI-NARY code by Ilijic et al. (2004). The method is designed to optimize simultaneously for the spectra of individual binary components and orbital elements of the system. The procedure we used here is similar to the one described in Tkachenko et al. (2014a,b), that is: in the first step, the orbital elements were derived from several spectral regions centred at prominent lines of neutral helium and doubly ionized silicon (He I $\lambda\lambda$ 4388, 4471, 4920, 5015Å and Si III triplet $\lambda\lambda$ 4553, 4568, and 4575 Å), and in the second step, the obtained orbital solution was used to separate the spectra of individual binary components in the entire wavelength range. In this particular case, the orbital elements used for the spectral separation are the ones obtained from the combined spectroscopic and photometric analysis (see Table 3). The wavelength range of the separated spectra covers several Balmer lines (H$_\delta$, H$_\gamma$, and H$_\beta$) and extends up 5300 Å. The whole red part of the spectrum was avoided in the disentangling because of numerous telluric contributions and a few stellar lines only present in that part of the spectrum. Instead, SPD was performed on individual stellar lines in the red part of the spectrum, that were advantageous to have for the analysis of chemical composition of the components (e.g. Si III $\lambda\lambda$ 5741 Å line and a few nitrogen, carbon, and aluminium lines nearby). The blue part of the spectrum was avoided because of uncertain continuum normalization. So, the spectral window that was finally used for the spectrum analysis covers the wavelength range between 4000 and 5300 Å. The final orbital solution was obtained by computing the mean orbital elements from all wavelength intervals mentioned above; the values are reported and compared to the previous findings in Table 3. All parameters are found to agree within the quoted error bars with the values reported by Herbison-Evans et al. (1971) and Shobbrook et al. (1972). Using the value of T$_0$ reported by Shobbrook et al. (1972) and the apsidal motion period $P_{aps} = 139 \pm 7$ yr derived by Aufdenberg et al. (2007), we calculate ω to be between 230° and 255° for the period of our observations. Thus, the value obtained by us for the longitude of periastron of 255.6 $\pm$ 12°.2 is in agreement with P_{aps} reported by Aufdenberg et al. (2007). Fig. 4 illustrates the final solution in terms of the computed RVs of both components,
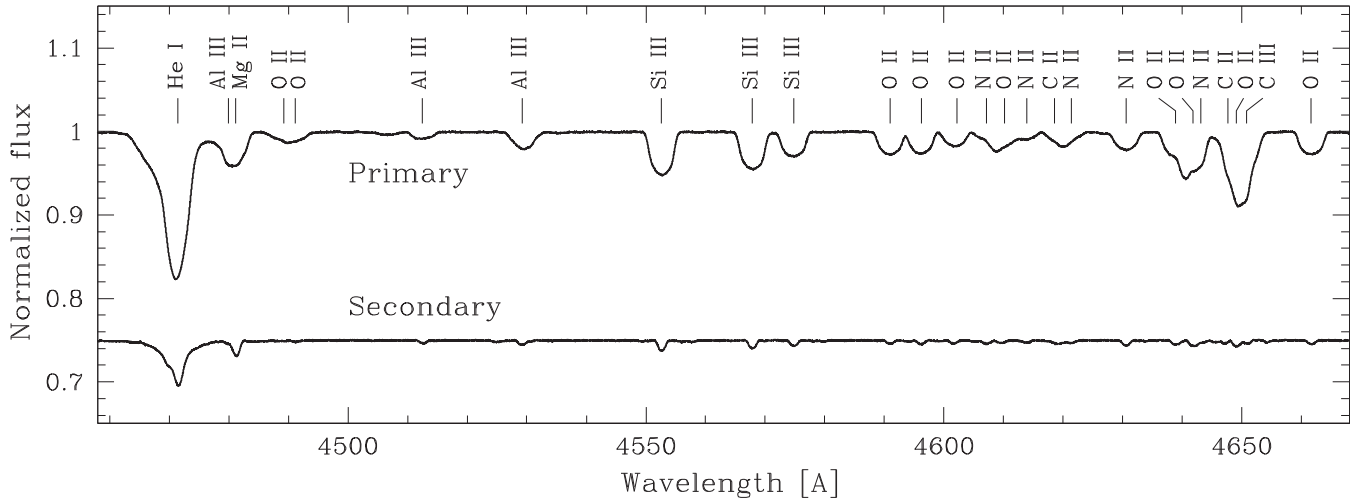
Figure 5. A portion of the separated (non-corrected for the individual light contributions) spectra of both stellar components of the Spica binary system. The spectrum of the secondary was shifted downwards by 0.25 (in continuum units) for clarity. The most prominent lines present in the spectra of both stars are also indicated.

and, at the same time, gives an impression about the orbital phase coverage achieved with our spectroscopic material.

Since the primary of Spica is known to be a variable star of β Cep type, and the SPD method assumes no variability intrinsic to either of the components of a binary system, the input data used for the SPD need some additional commenting. We used the approach adopted in Tkachenko et al. (2014b), that is we binned the original spectra with orbital period derived in Section 3. From a set of experiments, we found 25 orbital phase bins to be the optimal choice, which provided a minimum number of orbital phase gaps, and sufficiently uniform distribution of the spectra over the bins. There are several advantages of using binned data instead of the original spectra, provided a large number of spectra is available: (i) a significantly reduced number of input spectra for SPD (25 compared to the original 1731 measurements), which in turn reduces the computation time; (ii) a much higher S/N for each spectrum; and (iii) the oscillation signal is suppressed to a level that it has only a minor impact on the results of the disentangling.

A portion of the separated spectra of both components is shown in Fig. 5, along with identification of most prominent spectral lines found in the spectra of both components. The spectra suggest that both components are B-type stars with the primary component rotating significantly faster than the secondary. A detailed spectrum analysis of both binary components is presented in the next section.

5 SPECTRUM ANALYSIS OF BINARY COMPONENTS

Eclipsing binaries are a prime source of accurate masses and radii of stars, given high-quality photometric and spectroscopic data can be obtained for them. Moreover, the atmospheric parameters and chemical composition of individual stellar components of such systems can often be measured to a higher precision than for single stars of similar spectral type and luminosity class (see, e.g. Pavlovski & Hensberge 2005; Pavlovski & Southworth 2009; Tkachenko, Lehmann & Mkrtichian 2009, 2010; Tkachenko et al. 2014a). This becomes possible due to the fact that the surface gravity of a stellar component can be computed directly from its mass and radius, and thus fixed in the spectroscopic analysis. This removes the degeneracy between $T_{\rm eff}$ and $\log g$ from which the spectroscopic analysis of

OB-stars is known to suffer, leading to the measurement of accurate individual abundances. This is not the case for non-eclipsing systems, where the precision achieved on the fundamental atmospheric parameters and chemical composition of the components is comparable to the one expected for single stars. However, spectroscopic analysis still is superior to the analysis of broad-band photometry, in the sense that the atmospheric parameters measured from stellar spectra are more accurate than the values inferred from photometric data.

Before the spectra of individual binary components can be analysed to determine basic atmospheric parameters and individual abundances, they need to be renormalized to the individual continua of the component stars. This is done by means of the light ratio, which is often determined from photometric data for eclipsing binaries and by means of the constrained fitting (i.e. fitting for the light ratio simultaneously with other fundamental parameters; Tamajo, Pavlovski & Southworth 2011) for non-eclipsing systems. In the particular case of Spica, we fit for the light ratio and the other atmospheric parameters of the individual stellar components simultaneously, so that the light contribution of each of the stars is one of the output parameters from our spectrum analysis. The fundamental parameters and chemical composition of both stars were derived by fitting their disentangled spectra to a grid of synthetic spectra, based on the so-called hybrid approach. The latter assumes the usage of local thermodynamic equilibrium (LTE)-based atmosphere models and non-LTE spectral synthesis, in our case computed with the ATLAS9 (Kurucz 1993), and DETAIL (Butler 1984) and SURFACE (Giddings 1981) codes, respectively. Justification of such approach is discussed in Nieva & Przybilla (2007). The adopted spectrum analysis procedure is discussed in Tkachenko et al. (2014a,b) in full detail but here we summarize a few key points only: (1) the whole analysis is based on the method of spectrum synthesis where a grid of synthetic spectra is fitted to the observations. Not only this concerns the determination of the atmospheric parameters of the individual stellar components but also their chemical compositions; both stars exhibit significant line broadening in their spectra, so the method of spectral synthesis is superior for the determination of individual abundances compared to the equivalent width measurements which suffers from heavy blending of spectral lines. (2) The determination of atmospheric parameters such as $T_{\rm eff}$ and $\log g$, as

Table 4. Atmospheric parameters of both components of the Spica binary system. Equatorial velocities were computed under the assumption of coplanarity.

Parameter	Unit	Primary	Secondary
$T_{\rm eff}$	K	25 300 $\pm$ 500	20 900 $\pm$ 800
$\log g$	dex	3.71 $\pm$ 0.10	4.15 $\pm$ 0.15
$v \sin i$	km s^{-1}	165.3 $\pm$ 4.5	58.8 $\pm$ 1.5
$v_{\rm turb}$	km s^{-1}	5.0 $\pm$ 1.0	3.0 $\pm$ 1.0
Light factor	per cent	85.5 $\pm$ 1.5	14.5 $\pm$ 1.5
$v_{\rm eq}$	km s^{-1}	185.4 $\pm$ 9.2	65.9 $\pm$ 3.2

well as the individual light factors is largely based on fitting the Balmer lines (H$_\delta$, H$_\gamma$, and H$_\beta$). (3) Microturbulent velocities are determined by fitting selected oxygen lines requiring a null correlation between the individual abundances and the equivalent widths of the corresponding spectral lines. The lines selected are those from Simón-Díaz (2010). We also use silicon lines as an additional check of the reliability of the determined microturbulent velocity. The projected rotational velocities of the stars are determined by fitting the metal line spectrum of each of the components.

Tables 4 and 5 list the atmospheric parameters and individual abundances for both stellar components of the Spica binary system. The primary component is found to be hotter and more evolved than its companion, whereas both stars have the same chemical composition within the quoted error bars. The errors are 1σ uncertainties, that for individual abundances take into account line-to-line scatter and the error propagation from the atmospheric parameters. The spectroscopically derived effective temperature of the secondary and surface gravities of both stars are in good agreement with the corresponding values of $T_{\rm eff,2}$=20 585 $\pm$ 850 K, $\log g_1 = 3.75 \pm 0.11$ dex, and $\log g_2 = 4.15 \pm 0.16$ dex obtained from the light-curve fitting and the dynamical masses and radii of the stars, respectively. The same concerns light factors: the light-curve solution delivers contributions of 84.4/15.6 per cent for the primary/secondary, which is in agreement with the spectroscopic findings within about 1 per cent. Our atmospheric parameters are also in good agreement with the values reported by Lyubimkov et al.

(1995), who found $T_{\rm eff}$ = 24 700 $\pm$ 500/20 800 $\pm$ 1 500 K, $\log g$ = 3.7 $\pm$ 0.1/4.2 $\pm$ 0.2 dex, and $v \sin i$ = 161 $\pm$ 2/70 $\pm$ 5 km s^{-1} for the primary/secondary component. Any discrepancies between our parameters and those determined by Lyubimkov et al. (1995) can be attributed to the fact that, in the latter study, the analysis was based on the original, composite spectra of the binary. The approach implemented in the current study and that is based on the analysis of the disentangled spectra of both components is more accurate as it does not suffer from spectral line blending due to the contribution of a companion star.

The quality of the fit to three Balmer lines (H$_\delta$, H$_\gamma$, and H$_\beta$) in the spectra of both stars is shown in Fig. 6. A set of carbon and nitrogen lines in the spectra of both binary components is illustrated in Fig. 7, along with the theoretical spectra computed assuming different abundances of these elements. A significant difference in rotational broadening of the spectral lines of the stars is easily caught by eye, as well as the similarity in their chemical compositions. Finally, we note that chemical compositions of both stars found in this study agree within the error bars with both the cosmic abundance standard (Nieva & Przybilla 2012) and chemical composition of the Sun as derived by Asplund et al. (2009). An exception is the abundances of carbon and aluminium in the atmosphere of the primary component, which seem to be slightly overabundant given our 1σ uncertainties. We do not find any increase in the surface nitrogen abundance for either of the binary components, which puts both stars in the Group 1 of Hunter et al. (2008, Fig. 1). For the further analysis, we will assume solar chemical composition for both binary components, as the above mentioned deviations of carbon and aluminium found for the primary will not have any impact on the analysis outlined in the next sections.

6 FREQUENCY ANALYSIS AND MODE IDENTIFICATION

In this section, we address the question of the variability intrinsic to either of the binary components, that manifests itself in terms of the brightness and line profile variations. The results of spectroscopic mode identification are also presented and discussed.

Table 5. Photospheric abundances derived for both stellar components of the Spica binary system. Abundances are expressed relative to the abundance of hydrogen, $\log \epsilon(H) = 12.0$. The third and the fourth columns give the number of lines used and the difference between abundances of a binary component and those of the Sun, respectively. Present-day cosmic abundances from Galactic OB stars (Nieva & Przybilla 2012) are given in the fifth column. The last column lists the solar abundances from Asplund et al. (2009).

| El.	$\log \epsilon(X)$	N	$[X/H]$	OB stars	Sun
			Primary component		
He	10.97 $\pm$ 0.06	6	0.00 $\pm$ 0.06	10.99 $\pm$ 0.01	10.97 $\pm$ 0.01
C	8.19 $\pm$ 0.05	4	-0.20 ± 0.07	8.33 $\pm$ 0.04	8.39 $\pm$ 0.05
N	7.76 $\pm$ 0.04	17	-0.02 ± 0.07	7.79 $\pm$ 0.04	7.78 $\pm$ 0.06
O	8.72 $\pm$ 0.08	8	0.06 $\pm$ 0.09	8.76 $\pm$ 0.05	8.66 $\pm$ 0.05
Mg	7.50 $\pm$ 0.10	1	-0.03 ± 0.13	7.56 $\pm$ 0.05	7.53 $\pm$ 0.09
Si	7.41 $\pm$ 0.20	6	-0.10 ± 0.20	7.50 $\pm$ 0.05	7.51 $\pm$ 0.04
Al	6.20 $\pm$ 0.08	2	-0.17 ± 0.09		6.37 $\pm$ 0.04
			Secondary component		
He	10.98 $\pm$ 0.07	6	0.01 $\pm$ 0.07	10.99 $\pm$ 0.01	10.97 $\pm$ 0.01
C	8.26 $\pm$ 0.14	4	-0.13 ± 0.15	8.33 $\pm$ 0.04	8.39 $\pm$ 0.05
N	7.81 $\pm$ 0.19	17	0.03 $\pm$ 0.20	7.79 $\pm$ 0.04	7.78 $\pm$ 0.06
O	8.82 $\pm$ 0.23	8	0.16 $\pm$ 0.24	8.76 $\pm$ 0.05	8.66 $\pm$ 0.05
Mg	7.45 $\pm$ 0.16	1	-0.08 ± 0.18	7.56 $\pm$ 0.05	7.53 $\pm$ 0.09
Si	7.52 $\pm$ 0.24	6	0.01 $\pm$ 0.24	7.50 $\pm$ 0.05	7.51 $\pm$ 0.04
Al	6.16 $\pm$ 0.17	2	-0.20 ± 0.17		6.37 $\pm$ 0.04
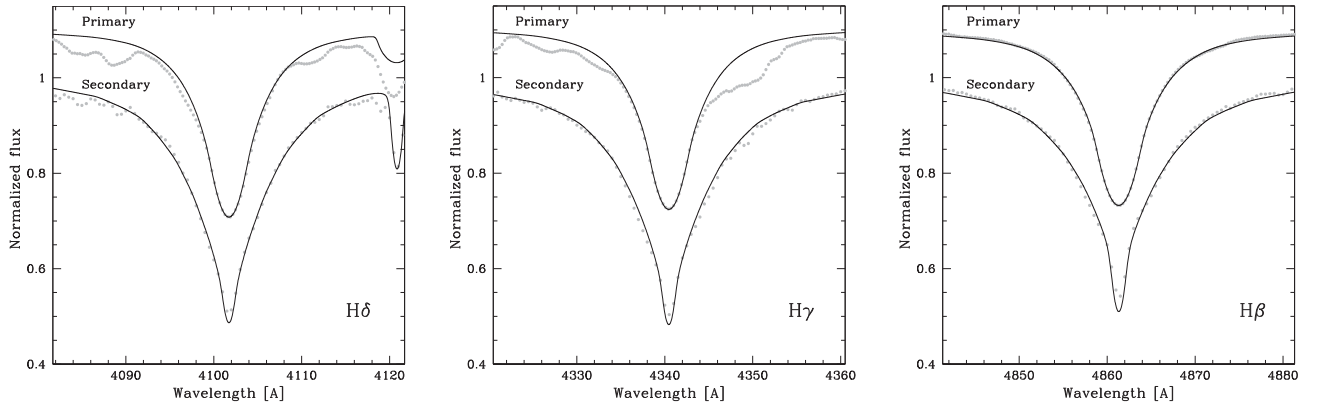
Figure 6. Best-fitting model (solid line) to the disentangled spectra (symbols) of both components of the Spica binary system. The spectrum of the primary was vertically shifted for clarity.
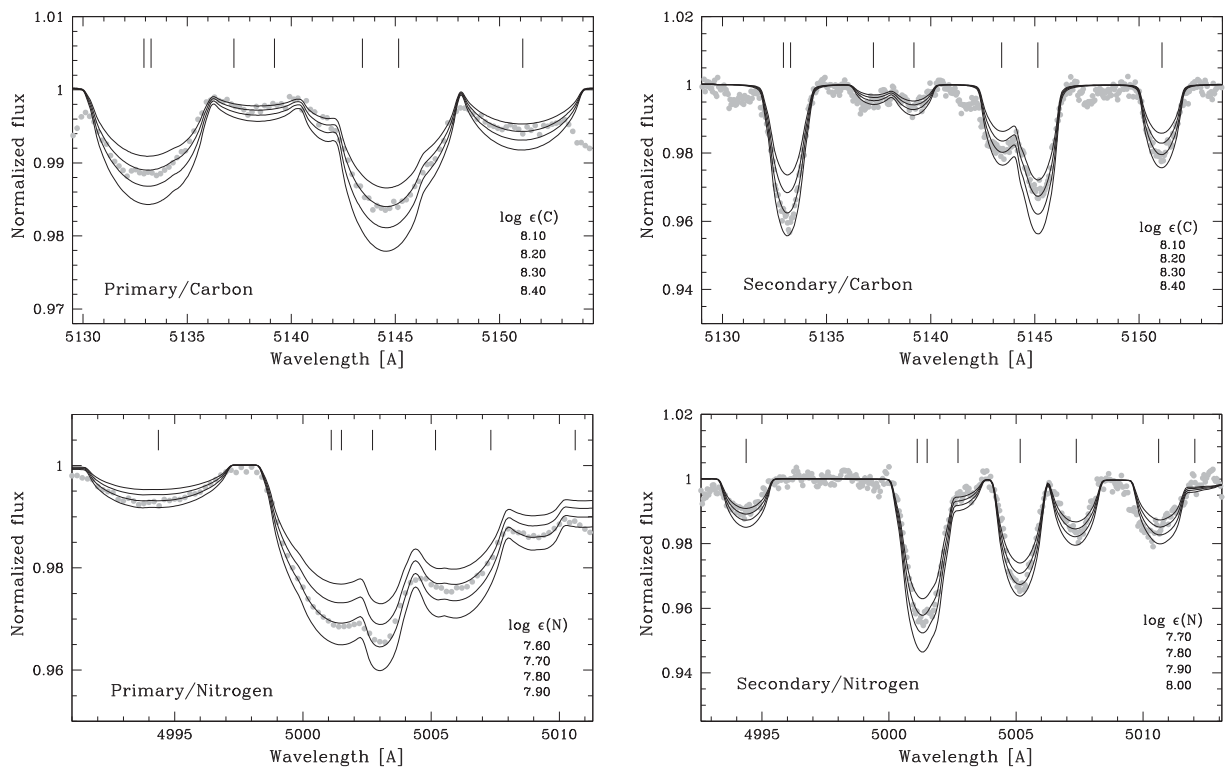

Figure 7. Fits of the theoretical spectra (lines) to the renormalized disentangled spectra of both stars (symbols) in the regions of carbon (top) and nitrogen (bottom) lines, and assuming different abundances of these elements. The columns (from left to right) refer to the primary and secondary component; the assumed abundances are indicated in the plot, where the smallest number corresponds to the weakest line. Note different X and Y scales for the primary and secondary which is due to large difference in $v \sin i$ values of the two stars.

6.1 Previous work

The intrinsic variability of the primary component of Spica was extensively studied in the past. Shobbrook et al. (1969) were the first to report on the detection of light variations intrinsic to the evolved primary with frequency of $\sim$5.75 d^{-1} (66.53 µHz). The variability has been attributed to a radial pulsation mode, thus the star has been classified as a β Cep-type variable. Smak (1970) came to the same conclusion and reported about a steady decrease of the dominant pulsation period at a rate of about 5 s per century. Shobbrook et al. (1972) investigated the system based on newly obtained photometric and spectroscopic data and confirmed the primary to be a variable star with the dominant frequency of

$\sim$5.75 d^{-1} (66.53 µHz). However, the authors found the pulsation mode to be variable in amplitude with the variability being random. A second pulsation mode was detected at a frequency of $\sim$3.97 d^{-1} (45.93 µHz) in the RV data and interpreted as the fundamental radial mode. The dominant mode was proposed to be due to the first overtone radial pulsation. Odell (1980) studied the Spica system by means of theoretical models and found that the photometric, orbital, and pulsation characteristics of the star can only be reproduced with models computed with opacities increased significantly over the Cox-Stewart opacities (Cox & Stewart 1969). The author also found the $l = 2$ surface geometry to be the most likely for the observed dominant mode at $\sim$5.75 d^{-1}.

Table 6. Results of the frequency analysis. The Rayleigh limit amounts to 0.044 d^{-1} for the photometry and 0.008 d^{-1} for the spectroscopy. Errors in the amplitude are given in parenthesis in terms of last digits. The photometric frequencies which are in common with the spectroscopic ones are highlighted in boldface.

| | Photometry | | | | Spectroscopy | | | | | | | |
| | | (magnitude) | | | | Pixel-by-pixel (continuum units) | | | | RV (km s^{-1}) | | |
f_i	Freq (d^{-1})	Freq (μHz)	Amplitude	S/N	Freq (d^{-1})	Freq (μHz)	Amplitude	S/N	Freq (d^{-1})	Freq (μHz)	Amplitude	S/N
f_1	0.694	8.030	0.001 98(7)	6.9	3.001 (12f_{orb})	34.722	0.014(1)	10.8	2.998 (12f_{orb})	23.117	4.32(3)	12.1
f_2	0.638	7.382	0.001 14(7)	5.5	5.748	66.504	0.012(2)	7.4	5.751	66.539	1.93(3)	4.5
f_3	1.486	17.193	0.001 08(5)	5.0	0.252 (f_{orb})	2.916	0.011(1)	5.6	0.248	2.869	1.4	4.1
f_4	**0.254** (f_{orb})	**2.939**	0.000 83(5)	4.4	2.162	25.014	0.007(1)	4.0	–	–	–	–
f_5	0.741 (3f_{orb})	8.573	0.000 82(5)	4.1	–	–	–	–	–	–	–	–
f_6	**2.149**	**24.864**	0.000 63(4)	4.0	–	–	–	–	–	–	–	–
f_7	**5.755**	**66.585**	0.000 57(3)	5.5	–	–	–	–	–	–	–	–

Walker et al. (1982) investigated new spectroscopic data obtained at orbital phases of large RV separation of the components. The authors detected 'bumps' moving across line profiles of the primary, just in line with the expectations for non-radial pulsations.

A detailed study of the variability intrinsic to the primary component was performed by Smith (1985a,b). About 500 high resolution, high S/N spectra were collected and analysed in the region of the Si III triplet at λλ 4553, 4568, and 4575 Å. Clear, though low-amplitude, variability has been detected in the RV data of all three components of the triplet. The signal was found to be due to four modes, $f_1 \sim 3.68$ d^{-1} (42.58 μHz), $f_2 \sim 7.5$ d^{-1} (86.77 μHz), $f_3 \sim 0.49$ d^{-1} (5.67 μHz), and $f_4 \sim 2.99$ d^{-1} (34.59 μHz); no evidence of the previously reported radial mode with frequency of ~ 5.75 d^{-1} (66.53 μHz) was found in the data. From the spacings between individual 'bumps' detected in the silicon line profiles of the primary, the modes f_1 and f_2 were found to have geometries corresponding to $l = m = 8$ and $l = m = 16$, respectively. The author also claims that these two modes have the same, high radial order n. The third mode at 0.49 d^{-1} (5.67 μHz) was attributed to the spectroscopic analogue of the photometric ellipsoidal variability and identified as an $l = 2$ mode. It is worth noting that this variability was detected indirectly, as a perturbing agent on the $l = 8$ mode. Smith (1985a) concluded that the system has achieved angular momentum equilibrium by eventually rotating bisynchronously, i.e. with the rotation period of the primary being half of the orbital period of the binary.

The $f_4 \sim 2.99$ d^{-1} (34.59 μHz) mode was analysed by Smith (1985b) in detail based on the data set obtained by Smith (1985a). The author found that the variability in question has very distinct behaviour: unlike non-radial pulsations that show continuously travelling bumps from blue to red wing of the line profile or vice verse, this variability is characterized by nearly stationary absorption like features in the wings. The amplitude of these features was found to be variable, making them to disappear and reappear again during the variability cycle. Smith (1985b) found that the variability due to the $f_4 \sim 2.99$ d^{-1} (34.59 μHz) mode can be well reproduced with a spherical harmonic function with the radial component of the displacement vector suppressed. Thus, the mode was found to have characteristics similar to those of toroidal modes, and was designated by the author as a 'quasi-toroidal mode'.

Harrington et al. (2009) presented an analysis of high-resolution spectra taken with the ESPADONS instrument attached to the Canada–France–Hawaii Telescope. The authors reported the detection of the lines of the secondary component in their spectra, and classified both components as B-type stars. The authors found all weak spectral lines in their spectra to display discrete narrow features

which could not be identified in He I and Balmer lines. The authors concluded that tidal flows exerted by the main-sequence secondary on the evolved primary are the main contributor to the short-term variability observed in the line profiles of the Spica system. Palate et al. (2013) arrived to a similar conclusion by analysing the data set obtained by Harrington et al. (2009) and using improved methodology. The conclusions of these two papers will be discussed in the context of our own results in the last section of the current study.

6.2 Most photometry

The photometric solution obtained in Section 3 was used to compute residuals from the original *MOST* light curve illustrated in Fig. 1 (top panel). For the extraction of individual frequencies, amplitudes, and phases from the residual signal, we used the Lomb–Scargle version of the discrete Fourier transform (DFT; Lomb 1976; Scargle 1982) and consecutive pre-whitening. A detailed mathematical description of the procedure can be found in Degroote et al. (2009).

The list of photometric frequencies extracted from the *MOST* light curve is given in Table 6 (first column, labelled 'Photometry'). The frequencies with values of S/N above 4 are listed only. Those which are in common with the spectroscopic frequencies are highlighted in boldface. Frequencies f_4 and f_5 are linked to the orbital frequency of the binary system and are due to imperfect removal of the orbital signal from the original light curve. Frequency f_7 has been previously reported in the literature as a radial pulsation mode with (randomly) variable amplitude (e.g. Shobbrook et al. 1969, 1972). Smith (1985a) reported that this frequency could not be detected in his spectroscopic data, but stressed that there is no reason to assume that the mode will not return eventually. All other frequencies detected by us in the *MOST* photometry are new and have not been reported in the literature before. Based on the results of our spectroscopic investigations (see below), we conclude that it is the primary component that is responsible for the photometric variability occurring on top of the orbital signal.

6.3 High-resolution spectroscopy

Our very first exercise with the spectra was to figure out which of the stars is intrinsically variable in the system. To do so, we have selected all individual spectra in a narrow range of orbital phase to make sure that all dynamics we see in the line profiles is due to variability intrinsic to either of the binary components and not due to the orbital motion within the system. Also, if all variability was due to tides and/or tidally locked (see, e.g. Harrington et al. 2009;
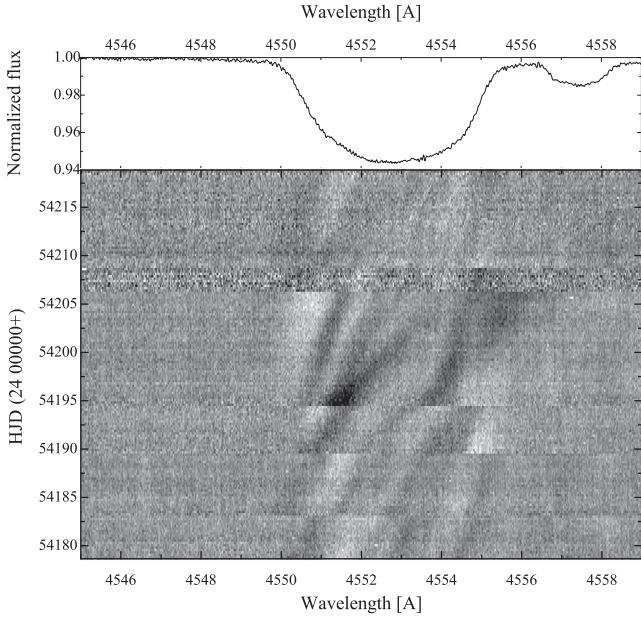
Figure 8. Top: average profile of the Si III λλ 4552.6 Å line computed from the time series of 162 composite spectra taken within narrow range in orbital phase. Bottom: time series of the residual spectra obtained after subtraction of the average profile. The grey-scale represent the residual intensity at each wavelength pixel.

Table 7. Fundamental stellar parameters of both components of the Spica binary system derived from the combined photometric and spectroscopic solution.

Parameter	Unit	Primary	Secondary
Mass, M	$M_\odot$	11.43 ± 1.15	7.21 ± 0.75
Radius, R	$R_\odot$	7.47 ± 0.54	3.74 ± 0.53
Luminosity, $\log L$	$L_\odot$	4.312 ± 0.095	3.353 ± 0.181
Effective temperature[a], T_{eff}	K	$25\,300 \pm 500$	$20\,900 \pm 800$
Surface gravity[a], $\log g$	dex	3.71 ± 0.10	4.15 ± 0.15

[a]Adopted from spectroscopy (see Table 4)

'equilibrium' tidal mode, which is basically a spectroscopic equivalent of the photometric ellipsoidal variability. This type of signal was also theoretically predicted by Harrington et al. (2009) to occur in the Spica system due to the tidal flows exerted by the components on each other. Our test with the real data shows that the signal at low-order harmonics of the orbital frequency is easily introduced into the data artificially, when the contribution of the secondary component is taken into account inappropriately, one way or the other.

The individual frequencies have been extracted from both RVs (computed as the first-order moment of the spectral line) and the line profiles themselves, using DFT and a consecutive pre-whitening procedure as implemented in the FAMIAS (Zima 2008) software package. Following the procedure described in Tkachenko et al. (2014a), the DFT was computed up to the Nyquist frequency, the amplitudes and phases were optimized at each step of the pre-whitening procedure while keeping the frequency values fixed, and the frequencies were accepted as significant ones if their S/N was higher or equal to 4 (Breger et al. 1993). For the analysis, we used the Si III triplet λλ 4553, 4568, and 4575 Å, but neglected all other lines potentially sensitive to non-radial pulsations (like He or Mg lines), because of high degree of their blending due to the rapid rotation of the star. The final list of frequencies is given in the second column of Table 6, labelled 'Spectroscopy'. Frequencies $f_2 \sim 5.75$ d^{-1} (66.53 μHz) and $f_3 \sim 0.25$ d^{-1} (2.89 μHz) were found both in the RVs and in the line profiles themselves, and agree within the error bars with the frequencies f_7 and f_4 detected in the photometric data. As it has been discussed in the previous section already, the former is likely a radial mode whereas the latter is the orbital frequency. There is a frequency, $f_1 \sim 3.00$ d^{-1} (34.71 μHz), that shows up in both spectroscopic observables, but could not be detected in the *MOST* photometry. This one is close to the 12th harmonic of the orbital frequency and is thus a good candidate for a mode excited by means of the dynamical tides expected to occur in eccentric binary systems. The same frequency was detected by Smith (1985a) in his spectroscopic data and explained in terms of a tidally forced 'quasi-toroidal' mode (Smith 1985b). The last frequency, $f_4 \sim 2.16$ d^{-1} (24.99 μHz), could be detected in the line profiles but not in the RV data, and has a low amplitude both in the spectroscopic and the photometric data.

We used FAMIAS to identify all three modes, f_1, f_2, and f_4, detected in our spectroscopic data. For that, we used the Fourier-parameter fit method (FPF; Zima et al. 2006), which is best suitable for mode identification in rapidly rotating stars. Identification of pulsation modes requires a knowledge of fundamental stellar parameters like mass, radius, effective temperature, surface gravity, etc. These were set to the values obtained from our combined photometric and spectroscopic solution, as summarized in the third column of Table 7. The individual masses and radii of the stars were computed from binary dynamics and we refer the reader to Tkachenko et al. (2014b,
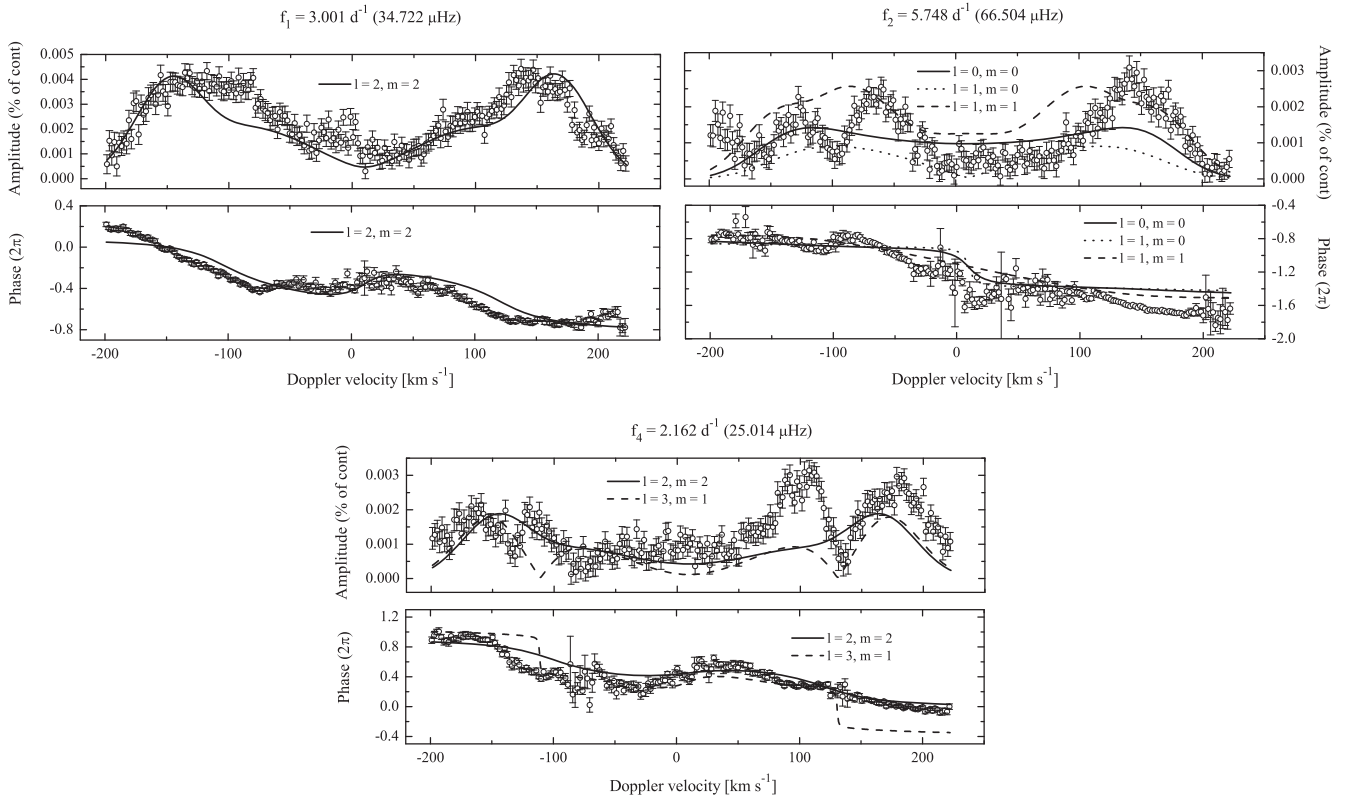
Palate et al. 2013), one would expect the signal to be repetitive with orbital cycle, i.e. nearly the same line profile pattern would be observed at a given orbital phase every orbital cycle (see Harrington et al. 2009, Fig. 6). We did the above mentioned exercise for both quadratures, where the spectral features of the two stars are well separated in wavelength. Since the obtained results are essentially the same for both orbital phases, we illustrate only one of them in Fig. 8. The top panel shows the average Si III λλ 4552.6 Å line, where the contribution of the secondary can be clearly distinguished from the one of the primary. The bottom panel illustrates a time series of the residual profiles obtained by subtracting the average profile from the individual spectra. There are 162 spectra shown in total; all of them were used to compute the average profile shown in the top panel. One can clearly see bumps moving from blue to red wing of the profile of the primary component, the signal typical for non-radial pulsations. There is no variability in our data that could be attributed to the secondary component.

In the next step, we used the disentangled spectrum of the secondary obtained in Section 4 to subtract the contribution of this star from the composite spectra of the binary. To test how good the removal of the secondary's contribution is, we did the frequency analysis of two different sets of the residual spectra: (i) all 1731 spectra; (ii) excluding the spectra where the lines of the secondary component merge with the lines of the primary. The goal of this exercise was to check which spurious frequencies will appear in the data due to the imperfect subtraction of the contribution of a companion star from the composite line profiles. We found that the frequencies at two and three times the orbital frequency (the second and the third harmonics of f_{orb}) show up in the first data set while they could not be detected in our second, orbital phase restricted data set. Thus, we conclude that these two frequencies are not real, and base our further analysis on the second set of 716 spectra. Interestingly, Smith (1985a) reported on the detection of $2f_{orb}$ periodicity in his spectra, and attributed it to an $l = m = +2$

Figure 9. Amplitude and phase distributions across the line profile for three pulsations modes: $f_1 = 3.001$ d^{-1} (top left), $f_2 = 5.748$ d^{-1} (top right), and $f_4 = 2.162$ d^{-1} (bottom). The best-fitting models are overplotted with the lines of different style; the corresponding mode geometry is indicated in each subplot.

Section 5) for any details. The luminosities were computed from the dynamical radii and effective temperatures of stars. In the first step, the modes were identified independently of each other, that is each time the star was treated as a mono-periodic pulsator. This often allows us to narrow the range in free parameters, particularly in l and m quantum numbers, which in turn significantly reduces the calculation time when the multiperiodic solution is searched for. To provide sufficient spatial resolution, we divided the stellar surface into 10 000 segments. At each iteration step, the amplitude and phase distributions across the profile were optimized along with the zero-point profile. Besides the l and m quantum numbers and intrinsic amplitudes of the modes, the intrinsic width of the Gaussian profile σ, projected rotational velocity of the star $v \sin i$, and the inclination of its rotational axis $i_{\rm rot}$ were set as free parameters. Since FAMIAS assumes an alignment between rotation and pulsation axes, it is possible to check for possible spin-orbit misalignment by keeping $i_{\rm rot}$ as a free parameter. Fig. 9 illustrates the distributions of amplitude and phase across the line profile for all three modes: $f_1 = 3.001$ d^{-1} (top left), $f_2 = 5.748$ d^{-1} (top right), and $f_4 = 2.162$ d^{-1} (bottom). The best-fitting models with χ^2 values below 20 are overplotted with the lines of different style; the corresponding mode geometries are indicated in the plots. Such large values of χ^2, that are obviously linked to the inconsistency between the model and observations in Fig. 9, can be attributed to the fact the high-order rotation effects are not taken into account in the FAMIAS model. The $f_1 = 3.001$ d^{-1} (34.722 µHz) mode is unambiguously identified as an $l = m = 2$ mode. No unique solution could be found for the modes f_2 and f_4, though the range in both quantum numbers is well constrained: we find that the former mode is likely a radial or $l = 1$ mode, while the latter is either $l = 2$ or 3 mode. All our best so-

lutions with χ^2 values below 20 suggest a range in the inclination angle of rotation axis $i_{\rm rot}$ between $53°$ and $66°$. This value is in good agreement with the orbital inclination of $i_{\rm orb} = 63°.1$.

7 EVOLUTIONARY MODELS

The MESA stellar structure and evolution code (Paxton et al. 2011, 2013) was used to compute evolutionary models for both components of the Spica system. Given that the secondary component rotates at about 10 per cent of its critical velocity, we have chosen to compute non-rotating models for this star. Contrary, the primary is found to rotate at ~30 per cent of its break-up velocity, and thus the rotation could not be neglected in the evolutionary model calculations for this binary component. The initial abundance fractions $(X, Y, Z) = (0.710, 0.276, 0.014)$ are those from Nieva & Przybilla (2012), in agreement with the spectroscopic findings (cf. Section 5). Convective core overshoot is described with an exponentially decaying prescription of Herwig (2000). The Ledoux criterion is used in the convection treatment. The OPAL opacity tables (Iglesias & Rogers 1996) and MESA equation of state are used.

Fig. 10 illustrates the position of both stellar components of the Spica system in the $T_{\rm eff}$–$\log g$ diagram. The error bars are those obtained from 1σ combined spectroscopic and photometric uncertainties (cf. Table 4). The evolutionary tracks are shown with solid lines for dynamical masses of both stars and the corresponding error bars (cf. Table 7). The tracks were computed for the overshoot parameter $f_{\rm ov} = 0.01$ ($\alpha_{\rm ov} \approx 0.1$ H$_p$); we also show the track computed with $f_{\rm ov} = 0.03$ ($\alpha_{\rm ov} \approx 0.3$ H$_p$) for a single mass value to illustrate the effect of overshoot on the evolutionary path of the star. Dashed lines show isochrones corresponding to 11.5 (bottom),
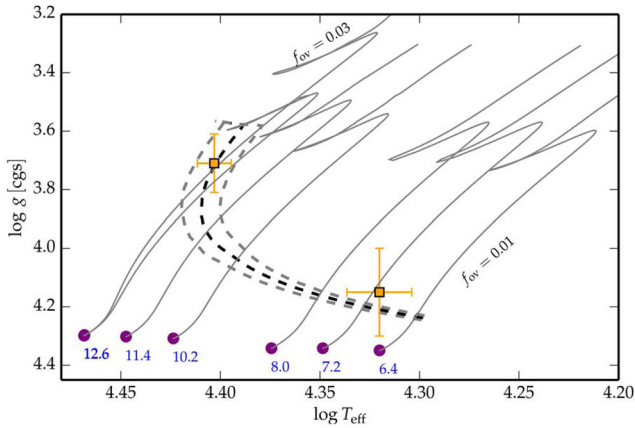
Figure 10. Location of the primary and secondary components of the Spica system in the $T_{\rm eff}$–$\log g$ Kiel diagram, along with the MESA evolutionary tracks. A track corresponding to a higher overshoot is shown for one selected mass to illustrate that it is impossible to constrain overshoot parameter $f_{\rm ov}$ from the models due to large error box in the determined fundamental parameters. Dashed lines show three isochrones corresponding (from bottom to top) to 11.5, 12.5, and 13.5 Myr

12.5 (middle), and 13.5 (top) Myr. The latter were computed assuming overshoot of $f_{\rm ov} = 0.01$. We find that the position of the unevolved secondary agrees very well with its dynamical mass evolutionary track. The same holds for the primary when the error bars on the mass, $T_{\rm eff}$, and $\log g$ of the star are taken into account. The positions of both stars are in good agreement with the isochrone corresponding to 12.5 Myr. By taking into account the errors on $T_{\rm eff}$ and $\log g$ for the primary component, we estimate the accuracy for the age to be of ± 1 Myr.

8 SUMMARY AND DISCUSSION

In this paper, we presented a detailed analysis of the Spica close binary system, based on high-resolution spectroscopy obtained with the CORALIE spectrograph and space-based photometry gathered with the *MOST* mission. In total, 1731 spectra and ∼23 d of nearly continuous photometric measurements have been analysed with the state-of-the-art modelling techniques. We found that the Spica system is close to showing a grazing secondary eclipse, the fact exciting by itself but hardly helpful for the analysis in terms of a better precision on the fundamental parameters of the component stars. Both binary components are found to have similar chemical composition consistent with the cosmic abundances derived from Galactic OB stars (Nieva & Przybilla 2012).

A comparison of the positions of both stars in the $T_{\rm eff}$–$\log g$ diagram with the MESA evolutionary models reveals a good agreement for the secondary component. This result differs from the one obtained by us for the V380 Cyg (Tkachenko et al. 2014a) and Sigma Scorpii (Tkachenko et al. 2014b) systems, where the unevolved secondary components were found to show significant discrepancy between their evolutionary and dynamical masses. A small mass discrepancy is not excluded for the primary component of Spica, though no definite conclusion can be drawn on this aspect because of rather large uncertainty of about 10 per cent in the stellar mass.

Contrary to Harrington et al. (2009) and Palate et al. (2013) suggesting that the line profile variations observed in the primary component can be naturally explained in terms of surface tidal flows exerted on it by the secondary, we find a clear evidence of non-radial pulsation modes in the system. One of the modes is interpreted by

us as being excited through a resonance between the free oscillation of the primary and the dynamical tides in the binary system. If confirmed with future observations, the Spica system will be the first massive binary (with the mass of the pulsating component larger than 5 M$_\odot$) in which tidally induced pulsations have been detected. Unfortunately, our attempt to carry out detailed asteroseismic modelling for the primary component of the Spica system was unsuccessful due to insufficient frequency resolution achieved with our data. In the result, several tens of models with χ^2 values below 1 were found when attempting to fit the observed frequencies, implying that the actual errors on individual frequencies are larger than the difference between the observed and theoretical values. The corresponding models cover entire parameter range in the fundamental stellar parameters such as the effective temperature, surface gravity, mass, radius, etc., implying that detailed asteroseismic analysis is not feasible with the data set we currently have. An accumulation of additional spectroscopic material would help to increase the frequency resolution, and thus would make the seismic analysis feasible for the primary component of Spica.

The mass discrepancy problem remains an unresolved issue in the massive binary research area for at least a few decades. It clearly points to some shortcomings in the current theories of stellar structure and evolution since the masses of the component stars measured from binary dynamics are model-independent values. As of today, the mass discrepancy problem, one way or the other, was addressed in several studies (e.g. Burkholder, Massey & Morrell 1997; Pavlovski et al. 2009; Garcia et al. 2014; Tkachenko et al. 2014a,b). The majority of the studies reported on a significant discrepancy between the dynamical and evolutionary masses, in a very few cases, the models were successful in matching the dynamical masses of the component stars. Revealing the shortcomings in the current theories of stellar structure and evolution requires a statistically significant, homogeneously analysed sample of massive binaries, whereas currently the analysis methods as well as the evolutionary models used by different authors are quite diverse. Spica is the third massive binary system, after V380 Cyg and σ Sco, that has been analysed by us in a consistent, homogeneous way, using the same modelling tools as for the other two binaries. We will extend our sample of massive binaries by adding about a dozen of eclipsing systems that we have recently discovered in the Campaign 0 data of the K2 mission. More systems are expected to be found in other fields of view of the K2 missions as well. With a few dozens of the systems in total analysed in a consistent way, we will be able to get more insight into the nature of the mass discrepancy problem for massive stars.

identification results with the software package FAMIAS developed in the framework of the FP6 European Coordination Action HELAS (http://www.helas-eu.org/). AT dedicates this work to his grandfather, A. Solomchenko, who passed away in 2016 January. Based on data from the *MOST* satellite, a Canadian Space Agency mission, jointly operated by Dynacon Inc., the University of Toronto Institute for Aerospace Studies and the University of British Columbia, with the assistance of the University of Vienna.

REFERENCES

Aerts C., Christensen-Dalsgaard J., Kurtz D. W., 2010, Asteroseismology. Springer, Heidelberg

Asplund M., Grevesse N., Sauval A. J., Scott P., 2009, ARA&A, 47, 481

Aufdenberg J. P. et al., 2007, in Hartkopf W. I., Guinan E. F., Harmanec P., eds, Proc. IAU Symp. 240, Binary Stars as Critical Tools & Tests in Contemporary Astrophysics. Cambridge Univ. Press, Cambridge, p. 271

Breger M. et al., 1993, A&A, 271, 482

Brott I. et al., 2011, A&A, 530, A116

Burkholder V., Massey P., Morrell N., 1997, ApJ, 490, 328

Butler K., 1984, PhD thesis, Univ. London

Claret A., 2000, A&A, 363, 1081

Cox A. N., Stewart J. N., 1969, Nauchnye Informatsii, 15, 1

Degroote P. et al., 2009, A&A, 506, 471

Degroote P., Conroy K., Hambleton K., Bloemen S., Pablo H., Giammarco J., Prša A., 2013, in Pavlovski K., Tkachenko A., Torres G., eds, EAS Publ. Ser. Vol. 64, Setting a New Standard in the Analysis of Binary Stars. EDP Sciences, p. 277

Desmet M. et al., 2009, in Guzik J. A., Bradley P. A., eds, AIP Conf. Proc. Vol. 1170, Stellar Pulsation: Challenges for Theory and Observation. Am. Inst. Phys., New York, p. 376

Garcia E. V., Stassun Keivan G., Pavlovski K., Hensberge H., Gómez Maqueo Chew Y., Claret A., 2014, AJ, 148, 39

Giddings J. R., 1981, PhD thesis, Univ. London

Hadrava P., 1995, A&AS, 114, 393

Hambleton K. M. et al., 2013, MNRAS, 434, 925

Harrington D., Koenigsberger G., Moreno E., Kuhn J., 2009, ApJ, 704, 813

Herbison-Evans D., Hanbury Brown R., Davis J., Allen L. R., 1971, MNRAS, 151, 161

Herrero A., Kudritzki R. P., Vilchez J. M., Kunze D., Butler K., Haser S., 1992, A&A, 261, 209

Herwig F., 2000, A&A, 360, 952

Hunter I. et al., 2008, ApJ, 676, L29

Iglesias C. A., Rogers F. J., 1996, ApJ, 464, 943

Ilijic S., Hensberge H., Pavlovski K., Freyhammer L. M., 2004, in Hilditch R. W., Hensberge H., Pavlovski K., eds, ASP Conf. Ser. Vol. 318, Spectroscopically and Spatially Resolving the Components of the Close Binary Stars. Astron. Soc. Pac., San Francisco, p. 111

Kudritzki R.-P., 1980, A&A, 85, 174

Kurucz R., 1993, ATLAS9 Stellar Atmosphere Programs and 2 km/s grid. Kurucz CD-ROM No. 13. Smithsonian Astrophysical Observatory, Cambridge, p. 13

Lomb N. R., 1976, Ap&SS, 39, 447

Lyubimkov L. S., Rachkovskaya T. M., Rostopchin S. I., Tarasov A. E., 1995, Astron. Rep., 39, 186

Mathis J. S., Odell A. P., 1973, ApJ, 180, 517

Nieva M. F., Przybilla N., 2007, A&A, 467, 295

Nieva M.-F., Przybilla N., 2012, A&A, 539, A143

North J. R., Davis J., Tuthill P. G., Tango W. J., Robertson J. G., 2007, MNRAS, 380, 1276

Odell A. P., 1974, ApJ, 192, 417

Odell A. P., 1980, ApJ, 236, 536

Palate M., Koenigsberger G., Rauw G., Harrington D., Moreno E., 2013, A&A, 556, A49

Pápics P. I. et al., 2012, A&A, 542, A55

Pápics P. I. et al., 2013, A&A, 553, A127

Pavlovski K., Hensberge H., 2005, A&A, 439, 309

Pavlovski K., Southworth J., 2009, MNRAS, 394, 1519

Pavlovski K., Tamajo E., Koubský P., Southworth J., Yang S., Kolbas V., 2009, MNRAS, 400, 791

Paxton B., Bildsten L., Dotter A., Herwig F., Lesaffre P., Timmes F., 2011, ApJS, 192, 3

Paxton B. et al., 2013, ApJS, 208, 4

Prša A., Degroote P., Conroy K., Bloemen S., Hambleton K., Giammarco J., Pablo H., 2013, in Pavlovski K., Tkachenko A., Torres G., eds, EAS Publ. Ser. Vol. 64, Setting a New Standard in the Analysis of Binary Stars. EDP Sciences, p. 259

Scargle J. D., 1982, ApJ, 263, 835

Shobbrook R. R., Herbison-Evans D., Johnston I. D., Lomb N. R., 1969, MNRAS, 145, 131

Shobbrook R. R., Lomb N. R., Herbison-Evans D., 1972, MNRAS, 156, 165

Simon K. P., Sturm E., 1994, A&A, 281, 286

Simón-Díaz S., 2010, A&A, 510, A22

Smak J., 1970, Acta Astron., 20, 75

Smith M. A., 1985a, ApJ, 297, 206

Smith M. A., 1985b, ApJ, 297, 224

Tamajo E., Pavlovski K., Southworth J., 2011, A&A, 526, A76

Thompson S. E. et al., 2012, ApJ, 753, 86

Tkachenko A., Lehmann H., Mkrtichian D. E., 2009, A&A, 504, 991

Tkachenko A., Lehmann H., Mkrtichian D., 2010, AJ, 139, 1327

Tkachenko A. et al., 2014a, MNRAS, 438, 3093

Tkachenko A. et al., 2014b, MNRAS, 442, 616

Vogel H. C., 1890, The Observatory, 13, 367

Walker G. A. H., Moyles K., Yang S., Fahlman G. G., 1982, PASP, 94, 143

Walker G. et al., 2003, PASP, 115, 1023

Welsh W. F. et al., 2011, ApJS, 197, 4

Wilson R. E., 1979, ApJ, 234, 1054

Wilson R. E., Devinney E. J., 1971, ApJ, 166, 605

Zima W., 2008, Commun. Asteroseismol., 155, 17

Zima W. et al., 2006, A&A, 455, 235

This paper has been typeset from a TEX/LATEX file prepared by the author.